Chapter 1
Introduction

Microsystems, or microelectromechanical systems (MEMS), technology continues to grow rapidly by enabling ever emerging applications that demand diverse, versatile functionality. Microsystems refers to a class of sub-millimeter scale sensors and actuators coupled with signal processing capable of measuring physical and chemical changes or performing desired physical and chemical functions. Microsystem technology based on micro-scale mechanical transducers progressed because silicon (Si) possesses both favorable electrical and mechanical properties to create these micro-sensor elements. Although many types of materials, ranging from ceramics to polymers, have been explored as platforms for microsystem technology, Si is currently the dominant platform. Si microsystems leverage the highly-parallel batch fabrication paradigm that has made microfabricated silicon-based semiconductor electronics commercially viable. Furthermore, they have benefited from a large body of knowledge around Si masking and etching techniques, which make fabrication of complicated geometries possible. This has enabled the current pervasiveness of silicon microsystems and components; they range from accelerometers for automotive airbags and inertial sensing, gyroscopes in video game controllers, micro-mirrors for projection displays, injector nozzles for inkjet printer cartridges, and mechanical timing references and RF filters for communication systems.

Diverse functionality, enhanced performance, small form-factor, and batch fabrication capability are the primary driving forces to using micro-scale systems technology. Smaller size makes it possible for noninvasive integration to existing systems. Batch fabrication promises more functionality at competitive price points compared to more traditional manufacturing techniques. Enhanced performance comes from two aspects of microsystems. A more direct integration of the sense elements with their electronics reduces noise. Sensitivity is increased by being able to make delicate structures that are inherently more sensitive or by utilizing physical phenomenon that dominate the response of these micro-structures but not their macro-scale counterparts. Given the considerable success to date of silicon microsystems for improving performance of a variety of commercial sensors, research has looked to expand the application space into harsh environments, such as combustion control and chemical process monitoring [1]. This has elevated the need for

M.B.J. Wijesundara and R. Azevedo, *Silicon Carbide Microsystems for Harsh Environments*, MEMS Reference Shelf 22, DOI 10.1007/978-1-4419-7121-0_1,

being able to use material systems compatible with harsh enviroment conditions to create sensors that can be used in an even wider range of applications than silicon.

Silicon carbide (SiC) is a leading alternative to Si in any application in which the environmental temperatures or level of radiation would damage silicon electronics or temperatures and corrosion would damage silicon or polymer sensor elements. SiC, like silicon, is usable as a semiconductor electrical element. In addition, it possesses mechanical behavior that is comparable to silicon. At high temperature, silicon dramatically softens and dopants diffuse, changing electrical behavior. Conversely, SiC does not significantly soften even at 600 °C and has a very low diffusivity. SiC is also highly resistive to a wide range of chemicals and can withstand high-temperature oxidative environments. Despite the chemical resistance of SiC, silicon-compatible etching and polishing processes have been developed for SiC. This allows a similar degree of flexibility in layout as silicon or polymer MEMS. Because of its overall stability of mechanical and electrical properties at high temperatures along with a developed batch manufacturing infrastructure, SiC is poised to open up a host of harsh environment applications to microsystem technology [2, 3, 4, 5].

This book aims to put into context how SiC technology can play a role in enabling sensors for a wide range of harsh environment applications not currently served by Si technology. It will also provide an updated view of SiC technology from deposition techniques, electronic device and microstructure fabrication, and packaging. It will conclude with a discussion of challenges in putting these parts together into a complete harsh environment microsystem, highlighting important research gaps in order to help spur interest in these areas. It aims to provide a useful reference for the MEMS practitioner yet remain accessible to those who are new to the field of microsystem technology.

To set the context for the remainder of the book, the remainder of this chapter will outline several harsh environment application spaces before outlining what makes SiC the right material system for developing microsystem technology for these applications.

1.1 Harsh environment applications

Harsh environment conditions are identified as undergoing large temperature excursions or required to operate for extended time at high temperature, exposure to highly corrosive and erosive conditions, intense radiation exposure, and high shock or intense vibration. These conditions are common to combustion environments, certain forms of energy and chemical production, space exploration, military-grade vehicle control sensing, and munitions monitoring (Figure 1.1). Microsystems capable of operating in the above environments with a high degree of reliability, efficiency, and sustainability are categorized as harsh environment microsystems. To extend the existing Si- or polymer-based commercial technology and techniques to harsh environment applications, development of robust material systems and device

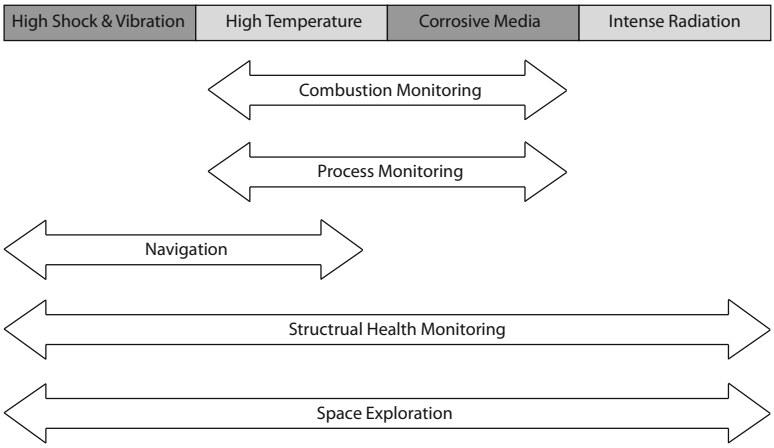

Fig. 1.1 Harsh environment conditions relevant to various harsh environment applications.

technology is needed. Requirements and benefits for each harsh environment application area are detailed next.

1.1.1 Combustion monitoring

Stringent environmental regulation and the demand for higher fuel economy require ever-increasing advances in combustion controls for automotive engines and gas turbines [6]. Combustion efficiency of automotive engines and gas turbines vary due to manufacturing discrepancy, aging of engine components, fuel properties, and intake air qualities (humidity and temperature) [7, 8]. For optimal efficiency and emission, precise control of temperature, pressure, air-to-fuel ratio, and ignition timing is required [9]. Traditional sensing methods are generally indirect with respect to the combustion event. Although they have been effective in further reducing emissions and improving fuel economy, further design optimization of these systems is seen to have limited additional improvements in emissions control and fuel efficiency. Therefore, research has shifted focus to active sensing and control of the combustion event in order to meet future regulation limits on emissions and higher fuel efficiency standards [8, 12].

Figure 1.2 schematically represents the overall concept of direct combustion monitoring. Increasing efficiency, lowering emission, and adapting fuel flexible technologies are key benefits that can be achieved through real-time monitoring and control of combustion events. Stoichiometric fuel burning and control of combustion temperature are required for reduction of CO, NO_x, and hydrocarbons. Figure 1.3 shows how precisely the air-to-fuel ratio has to be controlled to achieve maximum efficiency and low emissions. On-board real-time monitoring of the combustion event allows optimization of combustion based on current fuel properties, air

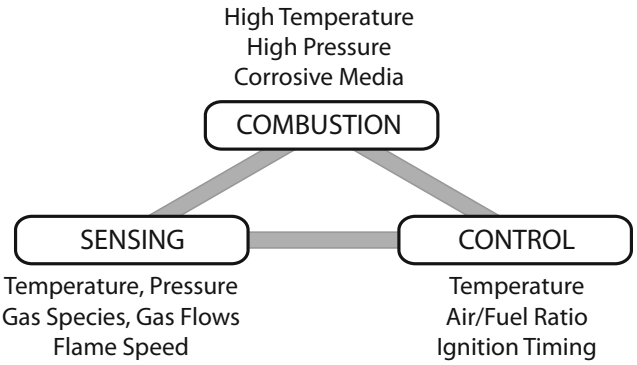

Fig. 1.2 Schematic representation of active closed loop combustion control through real time monitoring.

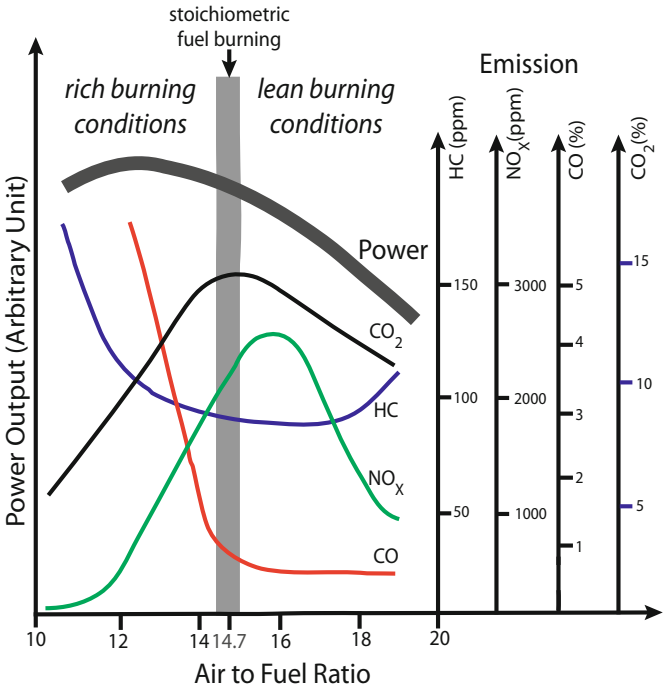

Fig. 1.3 Emission and power output of typical gasoline automotive engine with respect to air to fuel ratio. (Data from [9], [10], and [11] used to create the plot.)

quality, and engine conditions. Active control allows optimization of the combustion process at all times and under differing load conditions so that the ideal range for temperature, pressure, and fuel-to-air ratio can be maintained. This kind of system will also enable fuel flexible operation as the engine can optimize the combustion

Table 1.1 [1] Typical conditions and anticipated time of operation of combustion sensors for automotive and gas turbine applications (©Elsevier 1999), reprinted with permission.

Application	Temperature [°C]	Conditions	Time of Operation [hrs]
Gasoline engine	200-450	pressure, oxidative	4000
Diesel engine	200-450	pressure, oxidative	6000
Gas turbine	400-650	pressure, vibration, oxidative	10000

parameters suited for the particular fuel type regardless of slight variations in the fuel constituent.

In particular to automotive engines, combustion efficiency varies cylinder to cylinder, compromising the overall efficiency of the engine and increasing emissions [13]. This variation is attributed to factors such as injector and air intake variability and temperature variation. Thus, individual cylinder control has become a topic of major interest for engine development. One of the approaches widely discussed is the use of in-cylinder combustion monitoring with closed-loop combustion control. Because of the need to be as close to the combustion event as possible to achieve the highest benefit from closed-loop control, harsh environment sensors will play a critical role in achieving this task.

Gas turbine optimization for high efficiency and reduced emissions focuses on combustion instability and burn pattern. Active control with embedded feedback sensors that perform dynamic pressure and air-to-fuel mixture measurements as well as temperature mapping are needed to directly dampen unwanted combustion instabilities and optimize the burn pattern. Microsensors that can operate in combustion conditions permit incorporating these systems into combustion chambers without an adverse effect to turbine operation.

In order to achieve the forecasted need for improved efficiency and reduced emissions, sensors that can measure combustion parameters such as temperature, pressure, flame speed, and chemical species are needed. MEMS-based sensors are of considerable interest because their small form factor potentially allows them to be directly incorporated into the combustion environment with negligible perturbation to the combustion event and to the chamber infrastructure. However, these sensors must withstand combustion conditions such as temperature, mechanical loads (pressure, vibration), and chemically aggressive media while still being able to perform reliably for an extended period of time. Table 1.1 summarizes the typical conditions and anticipated time of operation of combustion sensors for automotive and gas turbine applications. As will be detailed later, these requirements exceed the limits of silicon-based microsensors and microsystems. Thus, alternative, high temperature materials are required.

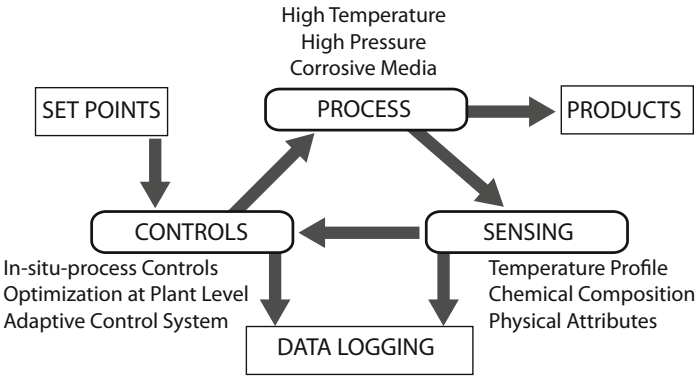

Fig. 1.4 Schematic flow of how sensor data can be used in industrial process control.

1.1.2 Process control

In any production environment, increasing production, maintaining quality, reducing operational cost, and minimizing waste are the common goals. Process quality monitoring through periodic sampling and product quality assessment leads to a lag before detecting out-of-tolerance conditions, which in turn results in increased costs due to production of inferior product that typically must be disposed of as well as wasted manufacturing resources. As with combustion monitoring, *in-situ* real-time monitoring of process parameters, process conditions, and product quality will allow active control that achieves the highest efficiency and standards because it is the most direct measurement of the system to be controlled [14, 15]. It also provides data logging capability for long-term planning as well as process and equipment improvements (Figure 1.4). Many industrial processes in energy and chemical production are extremely harsh. Sensors must survive these conditions for a extended period of time to be utilized in active control. If the sensors can also be made compact enough, it would be possible for direct implementation inside critical reactors and ancillary equipment. Microsystems can achieve the desired form factor. So harsh environment microsystem research is targeting improved chemical robustness to realize active control for these types of applications. Two major industries that can vastly benefit from harsh environment microsystem technology are oil exploration and extraction and chemical production.

1.1.2.1 Oil and Energy

Oil and gas extraction has changed tremendously as the demand for fossil fuels increases. For instance, petroleum wells have changed from simple vertical wells to more complex subsurface networks comprising of horizontal, multi-lateral, and multi-branched wells (Figure 1.5). This complexity has introduced new challenges

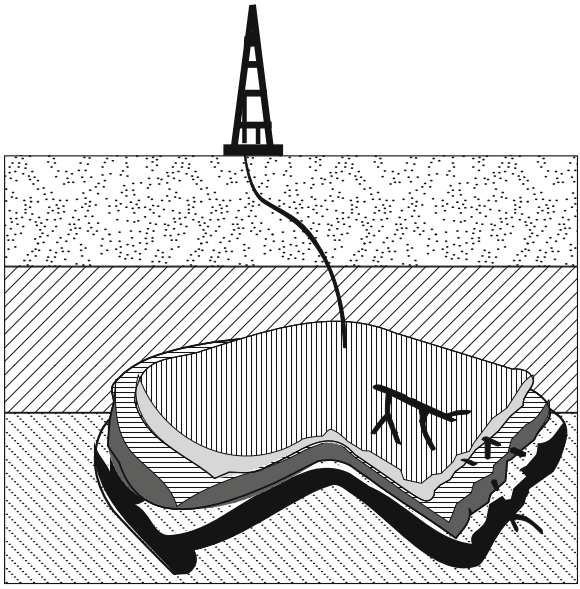

Fig. 1.5 Schematic representation of a multi-lateral, multi-branched oil well.

in reservoir management in order to increase oil and gas production, maximize recovery, and at the same time minimize operation cost.

The current practice of gathering down-hole information through periodic interrogation and data logging is costly and has a risk of damaging the well. Additionally, optimization of oil production is rather difficult. Down-hole sensors are still typically in the proposal or research stage. However, there are some limited deployments, such as the use of fiber Bragg grating sensors, to acquire dynamic and static conditions of the well [16]. Due to the complexity of these methods, there are ongoing efforts to develop better technology for distributed sensors throughout the well to get real time data on temperature, pressure, flow rates, and water content as well as distributed actuators to control fluid flow. The data from these sensors along with flow control systems will allow real-time optimization and improve tactical reservoir management and strategic planning. But the down-hole environment requires survival in liquid and often corrosive media as well as exposure to high pressures and temperature [17]. Given recent concerns with deep water drilling, distributed sensing may also provide another layer of safety to these types of installations. If these sensor and actuator modules can be controlled wirelessly, wide spread usage is expected; however, the distances and media involved are difficult challenges for reliable wireless communication.

1.1.2.2 Chemical Manufacturing

The traditional product control methodology often leads to sub-optimal equipment utilization, long delay time when transitioning product grades, and changes in product qualities at start-up and shutdown in many chemical industries. In part, the difficulty lies in indirect measurement techniques and associated lag time between the chemical process and sensor location because of limitations in sensor survivability.

Similar to oil well applications, integrated reactor sensors and feedback control units can detect changes at the precise moment and allow more instantaneous remedies, which will improve consistency of the product [18]. Real-time data is the key. Typical sensors that are needed in most chemical industries include optical properties, temperature, flow, pressure, chemical content, humidity, viscosity, and particulate and slag detectors.

In most chemical industries, severe processing environments require sensors that operate reliably at high temperature, high pressure and in corrosive conditions for active control of the process. These conditions can rapidly breakdown polymer-based sensors and can often corrode even silicon-based sensors as well, making certain direct reactor measurements impractical with existing technology. Furthermore, the operating temperatures may lead to premature failure or outright exceed the operating limits of silicon electronics, requiring remote sensor signal processing with respect to the reactor environment.

1.1.3 Military and Space Navigation

High precision navigation is a prerequisite for most military and aerospace launch vehicles. Real-time three-dimensional position data and precise time measurement along with thrust and trajectory controls are essential for successful mission completion [19]. This is true for both manned and intelligent unmanned operations including space shuttles, rockets, missiles, UAV, and even planetary probes like the Mars rover. Current inertial measurement units (IMUs), which incorporate gyroscopes and accelerometers with sense electronics to provide information on up to six degrees of freedom, work in conjunction with position control thrusters to provide the necessary functionality. The current units are large, heavy, and require a significantly large power source as well as bulky cooling systems. This is primarily due to high temperature and extreme shock and vibration environment typical in military and space applications. In most military and space applications, launch or landing impact can exceed 100,000 g; thus high g survivability is key [20, 21]. Space exploration missions additionally subject sensors to high levels of radiation and in some cases corrosive gases.

Silicon-based MEMS position sensing systems are being fabricated in an integrated fashion making these systems extremely small and low weight. Gyroscopes, accelerometers, and control electronics integrated into small IMUs not only decrease size and weight but also tend to reduce power consumption. This allows

these systems to be applied to new and existing systems with minimal intrusion to the infrastructure. Low power, smaller size, and reduced weight also allow applications in lighter, faster, and smaller-sized launch vehicles or aircraft critical for future combat and aerospace operations.

State-of-art silicon-based technology is not compatible with the operating conditions encountered by most of these systems without supporting infrastructure such as cooling, extensive packaging, and radiation shielding. These additional items add more volume and weight, reducing the inherent size and weight advantage of MEMS-based systems. Especially in the demanding field of space exploration, but even for more traditional military applications, all of these weight and size factors must be minimized in order to decrease the overall cost of the mission.

Hence, more robust systems that can also survive the application environment with a dramatically reduced supporting infrastructure are needed to maximize the benefit of payload reduction by adopting microsystem technology. If instead high temperature and shock resistant inertial navigation microsystems are developed that can in some cases be used directly, with no external cooling or sophisticated packaging, that in turn reduces weight, decreases complexity, and enhances reliability.

1.1.4 Structural Health Monitoring

All engineered structures undergo material and geometrical changes over time due to use, environmental effects, and manufacturing anomalies. The process of measuring these structural changes is referred to as structural health monitoring (SHM) [22]. The most common monitoring process involves periodic evaluation of structural properties; however, periodic evaluation provides limited knowledge. In the worst case, this can lead to unsafe conditions and loss of life. It also leads to unscheduled downtime and often extensive labor costs due to the unscheduled nature of the event. Most importantly, unanticipated failures can occur between inspection intervals. The real-time monitoring of in-service structures with less human intervention mitigates the shortcoming of periodic-inspection-based SHM [23].

A variety of sensors capable of continuous monitoring of structural response are commercially available. These are commonly piezoresistive, piezoelectric, or fiber-optic based. Real-time monitoring requires integrating these sensors and signal processing units into critical areas of the structure. The integration and networking complexity depends on sensor type, structure type, and its dynamic state. Additionally, the physical complexity of a structure as well as periodic maintenance, which may involve replacement of structural components, make wire based solutions less attractive or prohibitively costly. Combining SHM sensor nodes wirelessly is an important aspect of the system design.

The ideal wireless sensor network module for SHM should consume very little power, be small, be reliable, and be stable over long intervals, require no real maintenance, and be capable of operating in a wide array of environments. MEMS-based systems are drawing considerable attention due to their versatile functionality,

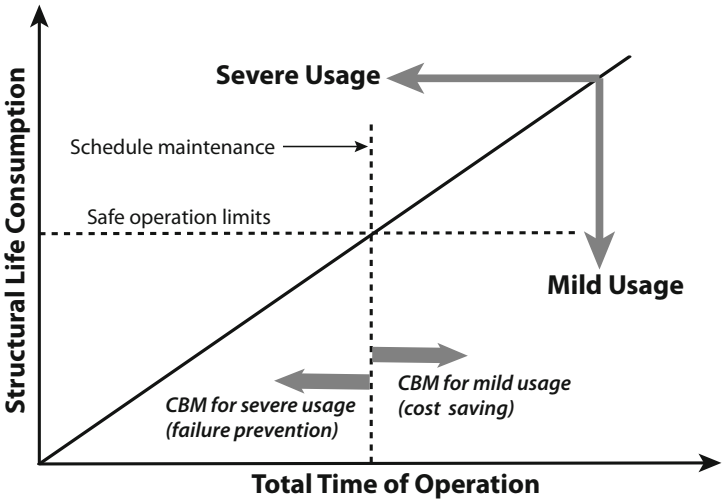

Fig. 1.6 Usage-based maintenance for failure prevention as well as for cost reduction. (Figure created using the concept presented in [24].)

low power requirement, small form factor, and high sensitivity. A small form factor sensor system with high sensitivity is very attractive since it can be installed onto many complex structures without the need to compromise the design of the original structure.

With continuous SHM, maintenance activities can be scheduled based upon actual conditions or usage of the system. This is called condition-based maintenance (CBM). Manufacturer recommended maintenance intervals can be either too aggressive based on actual use, leading to unnecessary costs, or too lenient in some circumstances, which can result in preventable failures. This generally becomes an issue because the manufacturer recommended intervals do not capture all the relevant operating conditions. For instance, sometimes early maintenance is necessary when heavy usage or environmental causes accelerate structural degradation. Or in-service structures can experience premature failure due to manufacturing imperfections, either in design or materials. Figure 1.6 graphically represents the advantage of usage-based maintenance for failure prevention as well as for cost reduction.

An extension of CBM is adaptive operation. The use of dynamic and static responses of in-service structures to optimize real-time operating conditions is called condition based adaptive operations (CBAO). As structures age, the likelihood of failure increases. Based on real-time structural health data, better operational conditions can be found to ensure safety and performance before maintenance is done. In this case, CBAO allows for safe extension of the maintenance interval when immediate down-time for the structure would prevent critical operations or interrupt sensitive missions. This can also extend to operating with known damage or under unusual external disturbances, in which case regular operational parameters have to

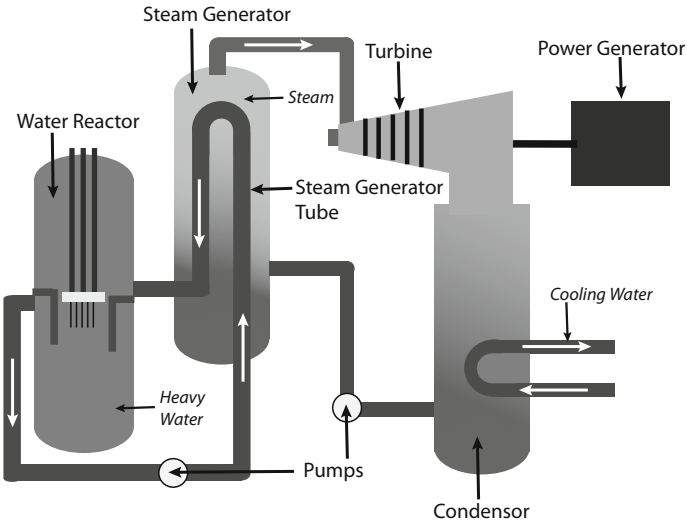

Fig. 1.7 Generalized architecture of a nuclear power plant.

be drastically adjusted to ensure safety until proper maintenance can be performed or the disturbance passes. In some situations, such as high-value military missions, it is desired to allow systems to push beyond their normal operating limits for limited intervals without sacrificing safety. For instance, monitoring structurally critical components for in-use deformation signatures can allow periodic relaxation of standard speed limitations during critical missions since real-time monitoring can facilitate development of less conservative safety factors. CBAO algorithms can use this information to both allow for overload conditions and adjust subsequent maintenance schedules for these equipment accordingly.

If these MEMS-based sensor systems were additionally capable of working in harsh environment conditions, these benefits could be extended from current work on bridges and buildings to specific critical needs in energy, avionics and aerospace, shipping, and chemical industries. Details of how harsh environment SHM would benefit these areas are discussed next.

1.1.4.1 SHM for Nuclear Energy Production

Figure 1.7 represents a generalized nuclear power plant. Pressure vessel and steam generator tubes are critical parts of a nuclear power reactor. Pressure vessels surround the nuclear reactor core that produces super-heated water. The steam generator tube exchanges this heated water from the core reactor side to the steam generation side for driving turbine generators. The structural integrity of both the pressure vessel and steam generator tube is vital as they contain water with radioactive fission products. Specifically, any leaks in the steam generator tubes could lead

to the escape of nuclear fission materials directly into the atmosphere in the form of steam. Pressure vessel and steam generator tubes degrade through many paths that include tube damage related to manufacturing process, general corrosion, pitting, stress corrosion cracking, or a combination of these mechanisms [26, 27]. Common methods of inspecting the structural integrity of steam generator tubes and pressure vessels include visual inspection, eddy current measurements, isotope analysis of steam, and helium leak tests. However, continual monitoring of load conditions on vulnerable areas, monitoring wall thickness changes, and tracking temperature profiles would increase the safely margin drastically and reduce downtime for inspections and repair. This is one area that can heavily benefit from harsh environment microsystems, especially systems that are temperature-, corrosion-, and radiation-hard.

1.1.4.2 SHM for Naval Vessels

Monitoring the hull structure is vital for any naval operation as most failures occur due to compromised hull integrity. Detection of hull thickness reduction rates, identifying localized corrosion, and tracking fatigue accumulation are highly critical for minimizing risk factors, optimizing operation, and improving ship fleet management [28]. Aging of naval vessels highly depends on operating conditions. For instance, vessels that operate in rough seas experience a higher degree of stress and fatigue compared to those in calm waters. Thus, continuous monitoring and data logging is important for maintenance scheduling. Real-time diagnosis of the ship hull response to rolling motion, wave slamming, and acceleration caused by ship movements and sea states allows adaptive control of vessel maintenance [29].

Sensors that are suited for naval structure monitoring include strain gauges for measuring structural flexure, pressure transducers for measuring emergence and slam, accelerometers for measuring vertical motion, and inclinometers to measure pitch and roll [30, 31]. Wireless sensors systems are ideal for naval vessels as many of the ship structures undergo frequently scheduled maintenance and parts replacement. MEMS are particularly attractive due to their small size, high sensitivity, and integration capability, which allows minimal effects on the structure and its functionality. However, the micro sensor systems applied to naval systems need to also withstand large temperature fluctuations and corrosive atmosphere present in naval environments.

1.1.4.3 SHM for Aerospace

The fuselage of an aircraft or spacecraft must withstand the loads anticipated during the service life of the aircraft regardless of the age [23]. Corrosion, erosion, stress-induced fatigue, and accidental damage are common causes of structural failure in airplane and space shuttle structures. Traditionally, inspections and maintenance are done at regularly scheduled intervals or when a problem is identified. These ap-

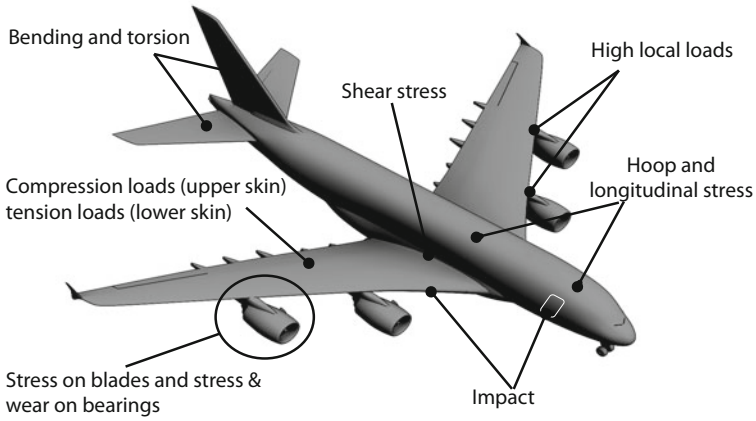

Fig. 1.8 [34] Loading points of aircraft structures (©ASME 2006), reprinted with permission.

proaches consume substantial resources and time. Furthermore, a catastrophic failure can occur, similar to that of Aloha 737, despite the above procedures, caused by a particular set of operational conditions not adequately captured by standard maintenance scheduling [33]. Aging of an aircraft component cannot be determined only by flying time or number of flights. It is also a function of operational conditions such as hard landings, severe turbulence, rough runways, and short distance flying. Real-time diagnostic and prognostic systems can vastly improve safety and reliability. As depicted in Figure 1.8, jet engine turbine components, wing structures, leading edges, landing gear, fuel tanks, and the fuselage are some of the critical component that can benefit from continual structural monitoring [34].

Even though some accelerometer and strain sensor solutions are proposed or currently being used, MEMS-based sensor platforms are desired due to small form-factor and low weight. Adapting harsh environment compatible sensor modules can further reduce weight by reducing cooling requirements or by allowing sensors to be integrated into critical high-temperature components like the aircraft engine. To measure the structural health of certain critical moving components such as turbine blades and bearings in the aircraft engine, it is imperative that these sensor modules be wireless [35].

Structural degradation of most space vehicles start from the moment of launch [36, 37]. For example, thermal protection shield damage of the space shuttle can occur during lift-off. Thus, space launch vehicles are prime candidates for SHM. As is the case for naval structures, the following sensors would provide much needed structural data on aerospace structures: strain, vibration (accelerometers), displacement, and temperature. Outer space opens up another aspect of harsh environment survivability because of the increased exposure to radiation and even larger temperature excursions. At the extreme end, the gamut of conditions are encountered

in NASA's Venus mission, which requires devices to operate around 500 °C at high-pressure conditions on the order of 90 atmospheres in the presence of carbon dioxide, sulfuric fumes, as well as chlorine and fluorine compounds. Silicon-based sensors and electronics are not expected to be suitable for such a mission without considerable infrastructure in place to protect them from the environment.

1.1.5 Space Exploration

Every space agency in the world has emphasized the need to reduce mission cost for future missions. The main way to accomplish this task is reduce the launch costs, which can be achieved simply by reducing the launch mass. For instance, reducing the launch mass of an interplanetary mission from 7800 kg to 750 kg will save nearly half a billion dollars just in the reduced cost of the launch rocket [38].

MEMS-based ultra-miniaturized systems for space applications have drawn considerable attention as a cost-saving measure by their considerable reduction in weight while being able to add new capabilities [40, 41, 42]. Low power requirements of these miniature systems also indirectly reduces mission weight by reducing the size of battery packs for instance. Currently, MEMS sensors are in early research or limited-use trials for many space expeditions. MEMS-based devices used in space missions include accelerometers, gyroscopes, pressure sensors, atomic force microscopes, and low-noise timing references for communications systems.

Even though current microsystems technology possesses the required maturity and reliability for many space applications, the limitations in intrinsic material properties hinder generalized application to many space environments. The systems applied into space applications should, as mentioned for SHM, have immunity to environmental conditions such as high temperature, high levels of radiation, and corrosive media [43, 44]. For current state-of-the-art microsystems technology, the cooling and heavy shielding infrastructure that is needed for environmental protection compromises the weight and size advantage over more traditional technologies. Thus, to fully tap into the weight and size advantages of microsystems, they should withstand the demanding conditions of space with little to no additional shielding or cooling components.

Some of the potential applications of harsh environment microsystems for space exploration have been discussed in previous sections such as navigation and structural health monitoring. At a component level, MEMS-based on-chip IMUs, RF switches and timing references, micro-valves, and micro-thrusters will enable new space mission scenarios. Applications such as micro-probes, micro-rovers, and aerobots will all benefit from the development of harsh environment microsystems technology. Furthermore, in addition to the weight-saving advantage of future manned and unmanned missions, new concepts like micro- and nano-satellite deployments will most likely depend on developing robust, reliable harsh environment microsystems that can meet the unique demands of space environments.

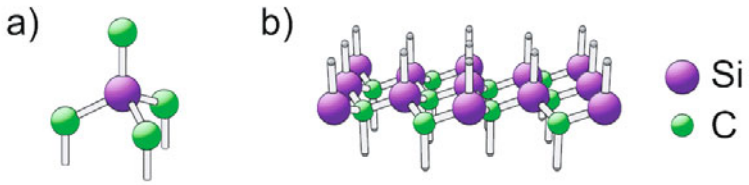

Fig. 1.9 [45] Atomic structure of SiC: a) tetrahedrally bonded Si-C cluster b) Hexagonal bilayer with Si and C in alternating tetrahedrally coordinated sites (©Springer 2004), reprinted with permission.

1.2 SiC properties

For the harsh environment applications outlined in the previous section, all the components of the microsystem must withstand either high temperature, high radiation, intense vibration, high G-shock, corrosive environments, or some combination. Thus, materials with robust chemical, electrical, and mechanical properties are needed. Silicon carbide (SiC) has been identified as the best suited material because of its unique materials properties. It is mechanically robust, chemically inert, and can be used as a semiconductor substrate for integrated circuits. Furthermore, SiC can be used to fabricate each and every component of the microsystem, namely electronics, sensors, and packaging.

1.2.1 SiC crystal structure

SiC can be found or produced in three forms: single crystalline, poly-crystalline, and amorphous. Depending on the device type and the functionality, all these forms can be useful in creating SiC microsystems. SiC substrates and electronics-grade epitaxial SiC are single-crystalline while most MEMS structures are fabricated using poly-crystalline SiC (poly-SiC). Amorphous SiC is useful for MEMS structures and isolation layers as well as device encapsulation.

Single-crystalline SiC exists in many different polytypes. However, most research has focused on just three types: 6H-SiC, 4H-SiC, and 3C-SiC (also known as β-SiC). In all polytypes, each silicon atom is bonded to four neighboring carbon atoms. Each carbon atom in turn bonds to four neighboring silicon atoms in a tetrahedral fashion (Figure 1.9a). These Si-C units are arranged in a hexagonal bilayer with Si and C alternately occupying sub-layers (Figure 1.9b). The stacking sequence of the Si-C bilayer with respect to the orientation of adjacent layer determines the polytype. 3C-SiC (cubic) is formed with an identical orientation of each bilayer and the atomic geometry is repeated every three layers along the c-axis of the crystal (Figure 1.10a). 4H-SiC (hexagonal) is formed by stacking blocks of two identically oriented bilayers to form the unit cell, but subsequent cells are rotated 60^o with re-

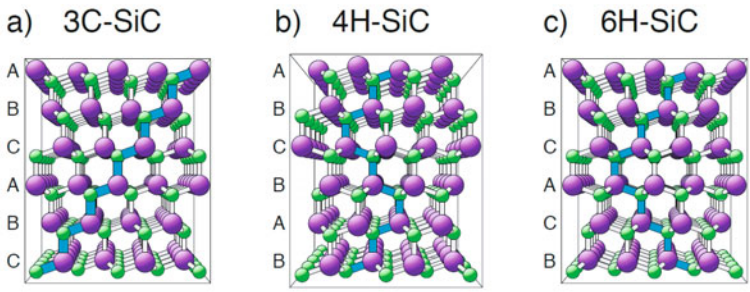

Fig. 1.10 [45] Crystal structure of different SiC polytypes displayed parallel to the $(11\bar{2}0)$ plane: (a) cubic 3C-SiC (β-SiC), (b) hexagonal 4H-SiC, and (c) hexagonal 6H-SiC (©Springer 2004), reprinted with permission.

spect to each other (Figure 1.10b). 6H-SiC (hexagonal) is formed with slabs of three identically oriented bilayers to form the unit cell. Again, the unit cell is rotated 60° with respect to the neighboring cell layers (Figure 1.10c).

Polycrystalline SiC, as the name implies, contains local regions of crystallinity; however, the crystals are not continuous throughout the layer. Adjacent islands of crystals may have different densities and crystal basal plane orientations. Poly-SiC is mostly produced as a thin film for MEMS device fabrication because of the reduced deposition temperatures required for poly-SiC fabrication over single-crystalline SiC. 3C-SiC is the most common polycrystalline polytype produced and can be deposited on various substrates including silicon and silicon carbide [46, 47]. Columnar or grain-type microstructure can be obtained by varying the deposition parameters. In addition to Si and C, poly-SiC may contain hydrogen or other residual elements depending the deposition methods.

Amorphous SiC is mainly use as a structural material for MEMS and encapsulation. The density and stoichiometry of the amorphous SiC are strongly dependent on deposition method and deposition parameters. Again, due to the lower deposition temperatures, residual elements such hydrogen and argon remain trapped in the film. Because of the lack of crystallinity, amorphous SiC acts as a dielectric.

1.2.2 Basic Chemical and Physical Properties

In this section, general physical and chemical properties are discussed. Electrical and mechanical properties are presented in following sections. SiC is a high temperature ceramic material. It sublimates at 2830 °C, which is very high compared to the melting point of silicon (1420 °C). The high temperature stability in the solid state is in part due to the extremely low diffusion rate in SiC. At high temperatures, most semiconductors undergo changes due to diffusion; however, significant diffusion does not occur until 1800 °C for SiC [48]. In addition to these properties, SiC is

also very chemically stable making it resistant to erosion and corrosion. Altogether, these properties make SiC a prime candidate for use in harsh environments.

SiC is inert to most chemicals at room temperature though some reactions can happen at very high temperatures [49]. For example, SiC does not react with potassium hydroxide (KOH) at room temperature but will readily react around 600 °C with molten KOH. SiC is resilient to most chemical etchants used in the standard microfabrication environment; however, amorphous SiC can be etched with 1:1 HF:HNO3. Because only amorphous SiC reacts with this acid mixture, not single crystalline SiC, the HF:HNO_3 mixture is used for selective etching of amorphous SiC over single crystalline SiC. A recent report shows that this acid mixture can slowly etch poly-SiC as well; the etch rate can vary from 0.01 to 5nm/min. The etch rate is inversely proportional to grain size [50].

For most application environments described in this chapter, a high oxidative environment is common. SiC is highly resilient to atmospheric conditions and forms a negligible amount of oxide on the surface. SiC undergoes oxidation with oxygen, carbon dioxide, and steam at high temperature. The oxidation reactions are shown in equation (1.1), (1.2) and (1.3) [69]:

$$SiC(s) + 3/2O_2(g) \rightarrow SiO_2(s) + CO_2(g) \tag{1.1}$$

$$SiC(s) + 3H_2O(g) \rightarrow SiO_2(s) + CO(g) + 3H_2(g) \tag{1.2}$$

$$SiC(s) + 3CO_2(g) \rightarrow SiO_2(s) + 4CO(g) \tag{1.3}$$

Many qualitative and quantitative studies have been done to compare the oxidation characteristics of SiC under atmospheric conditions and in hydrocarbon combustion environments. It is found that SiC forms a silicon dioxide passivation layer and the rate of oxidation formation is diffusion limited at temperatures below 1200 K. For example, heating of poly 3C-SiC at 1025 K in atmospheric air resulted in a 5 nm thick oxide layer during the first five hours [69]. Going to even higher temperatures does eventually lead to an oxidation condition that results in significant material loss in SiC. At temperatures above 1200 K (927 °C), which is beyond the harsh environment application space discussed previously, competing redox reactions can occur in the presence of hydrogen, CO, and vapor H_2O forming volatile SiO [52]:

$$SiO_2(s) + H_2(g) \rightarrow SiO(s) + H_2O(g) \tag{1.4}$$

$$SiO_2(s) + CO(g) \rightarrow SiO(s) + CO_2(g) \tag{1.5}$$

$$SiO_2(s) + H_2O(g) \rightarrow SiO(OH)_2(g) \tag{1.6}$$

$$SiO_2(s) + H_2O(g) \rightarrow SiO(OH)_4(g) \tag{1.7}$$

This reduces the surface SiO_2 layer thickness resulting in a linear oxidation rate.

When comparing the oxidation behavior of common MEMS materials such as single crystalline silicon, diamond-like carbon (DLC) film, and poly 3C-SiC film under oxidation conditions relevant to the harsh environment applications of interest (1025 K in atmospheric air), SiC films possess a relatively high oxidation resistance. Under the above conditions, 500nm DLC was burned out during the first 24 hours

Table 1.2 Electrical properties of Si, GaAs, 6H-SiC, 4H-SiC, and 3C-SiC [53, 68]. When values depend on orientation to the c-axis (parallel, ∥, or perpendicular, ⊥), both are listed.

Property	Si	GaAs	6H-SiC	4H-SiC	3C-SiC
Energy Bandgap [eV]	1.12	1.43	3.03	3.26	2.3
Thermal Conductivity [W/cm-K]	1.5	0.5	3.0-3.8	3.0-3.8	3-4
Intrinsic Carrier Concentration [cm^{-3}]	10^{10}	1.8×10^{6}	10^{-5}	10^{-7}	10
Saturated Electron Drift Velocity [10^7 cm/s]	1.0	1.2	2.0	2.0	2.5
Breakdown Field, Doping Conc. of 10^{17} cm^{-3} [MV/cm]	0.3	0.4	∥ 3.0 ⊥ 2.5	∥ 3.2 ⊥ 1.0	1.8
Electron Mobility	1200	6500	∥ 60 ⊥ 400	800	750
Relative Dielectric Constant	11.9	13.1	9.7	10	9.6

while silicon and poly-SiC makes 290 and 48 nm of oxide after 100 hours, respectively [69]. This clearly demonstrates the superiority SiC over these other MEMS materials.

1.2.3 Electrical

In this section, two aspects of electrical properties are discussed. First, semiconductor material properties are discussed in terms of electronics that can survive high temperature, high power handling, and high radiation fields. Second, electrical properties are discussed in terms of a transducer material for high temperature environments. Mostly 4H-SiC and 6H-SiC are discussed in regards to electronics, as they are the polytypes currently available in wafer form. Single-crystal SiC and poly-SiC will be discussed as a piezoresistive sensing materials. Table 1.2 summarizes the basic electronics properties of SiC in addition to other commonly used semiconducting materials for comparison.

1.2.3.1 High temperature electrical behavior of SiC

High temperature electronics operation requires thermal stability of electrical parameters of the semiconductor itself as well as the semiconductor device. Thus, both intrinsic properties of the semiconductor and the device architecture play a critical role in temperature stability. This section focuses only on the intrinsic material properties aspect.

In semiconducting materials, increased temperature leads to a decrease in the energy band gap and an increase in carrier concentration, which in turn adversely affects the device performance. Materials with high bandgap and low intrinsic carrier concentration are needed for high temperature electronics applications.

As shown in Table 1.2, SiC possesses a higher energy bandgap compared to the more widely used Si and GaAs. Figure 1.11 graphically represents the estimated energy bandgap of Si, GaAs, 4H-SiC, and 6H-SiC as a function of temperature. The

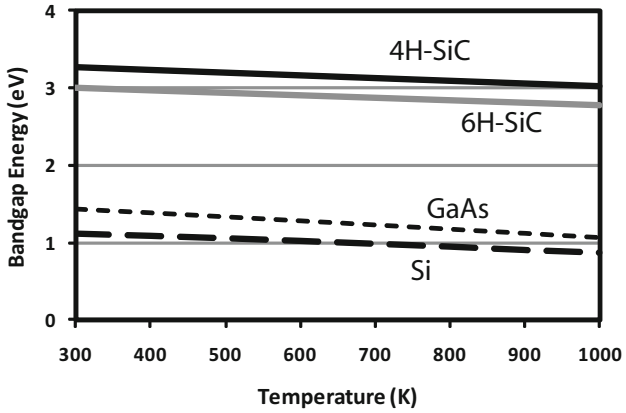

Fig. 1.11 Calculated energy band gap of Si, GaAs, and SiC as a function of temperature [54].

data clearly show a decrease in bandgap with increasing temperature. This bandgap reduction leads to larger intrinsic carrier densities, high leakage currents, poor junction rectification, and poor device isolation [54]. In comparison to Si and GaAs, both 6H-SiC and 4H-SiC retain a high bandgap value at even 1000 K, confirming SiC is better suited for high temperature operation.

Intrinsic carriers of semiconductors refers to thermal electrons and holes carriers present in the material at a given temperature. For proper operation of a semiconductor device, the intrinsic carrier density should be well below the intentional dopant-induced carrier density. For instance, the intrinsic carrier density of Si is 10^{10} cm^{-3} and well below the typical dopant-induced carrier densities for Si of 10^{14} to 10^{17} cm^{-3} at room temperature. For 6H-SiC, the intrinsic carrier density is 10^{-6} cm^{-3} and the typical dopant induced carrier density ranges from 10^{15} to 10^{17} cm^{-3} at room temperature; however, carrier concentration is strongly dependent on bandgap and temperature. The correlation of intrinsic concentration (n_i) and temperature is given by [54]:

$$n_i = [N_C N_V]^{1/2} exp[\frac{-E_g(T)}{2kT}] \tag{1.8}$$

where N_C and N_V are the number of carriers and vacancies respectively, $E_g(T)$ is the energy bandgap at a given temperature, and k is the Boltzmann constant.

As shown in Figure 1.12, the intrinsic carrier concentration of SiC stays well below allowable limits even at 1000K, allowing operation of SiC electronic devices at extremely high temperatures without suffering from intrinsic conduction effects.

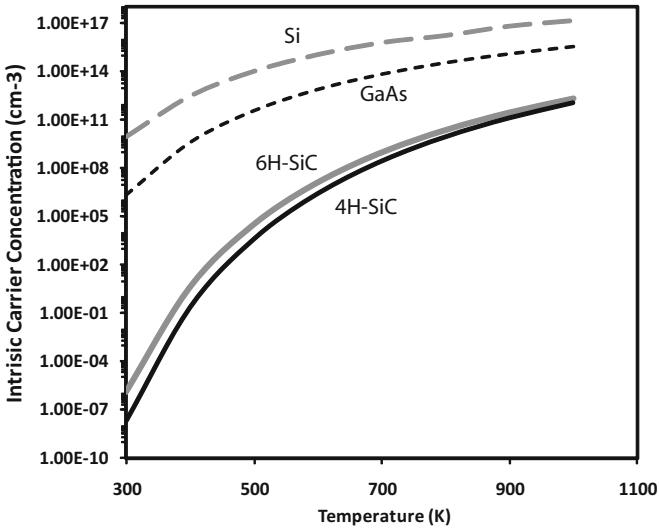

Fig. 1.12 Calculated intrinsic carrier concentration of Si, GaAs, and SiC as a function of temperature.

1.2.3.2 Wide-bandgap SiC for high power electronics

Solid-state semiconductor devices are being used or considered for power distribution and conversion. To fully tap the capabilities of solid-state devices, both materials and component level issues must be addressed. In this section, materials capability of SiC for power handling devices with comparison to common semiconducting materials will be discussed. More efficient high power electronics require low on resistance, low switching loss, high blocking characteristics, increased operating frequency, and high operational temperature capability. The primary material properties that improve these characteristics of high power solid state devices are large bandgap, high breakdown field, high saturated electron drift velocity, and high thermal conductivity.

SiC has a high breakdown field in comparison to silicon and gallium arsenide (Table 1.1), thus, SiC based power devices have higher breakdown voltages. A higher electric breakdown field also allows fabrication of device with thinner drift region.

The breakdown voltage (V_B) and the drift region width at a given breakdown voltage of a p-n diode can be approximated by equations 1.9 and 1.10, respectively [55]:

$$V_B \sim \varepsilon E_c^2 / 2qN_d \tag{1.9}$$

$$W(V_B) \sim 2V_B / E_c \tag{1.10}$$

Table 1.3 Comparison of breakdown voltage and drift region width of Si, GaAs, 4H-SiC and 6H-SiC.

Semiconductor	Si	GaAs	4H-SiC	6H-SiC
Breakdown voltage (V) for doping concentration N_d	$2.96 \times 10^{17}/N_d$	$5.76 \times 10^{17}/N_d$	$249 \times 10^{17}/N_d$	$274 \times 10^{17}/N_d$
Drift region width (cm) for breakdown voltage V_B	$6.67 \times 10^{-6} V_B$	$5.00 \times 10^{-6} V_B$	$0.67 \times 10^{-6} V_B$	$0.63 \times 10^{-6} V_B$

where ε is the permittivity ($\varepsilon = \varepsilon_r \varepsilon_0$), where ε_r is the dielectric constant and ε_0 is the vacuum permittivity) E_c is the breakdown voltage, q is the charge of an electron, N_d is the doping density. Using data from Table 1.2 and assuming the same doping density and drift region width, the breakdown voltage (V_B) of Si, GaAs, 4H-SiC, and 6H-SiC are shown in Table 1.3.

The data clearly shows that both 4H- and 6H-SiC devices have much higher breakdown voltages for a given doping concentration, and their drift regions are much thinner at a given breakdown voltage than their counterparts made from silicon and gallium arsenide. Thinner drift region yields lower resistance in the on state, resulting in much lower conduction losses. Moreover, SiC can be highly doped owing to its high breakdown field and can be utilized to further reduce the on state resistance. Reduction of on state resistance allows high power handling capability with better efficiency. As the device gets thinner, the storage of the minority carrier decreases, reducing the reverse recovery loss as well. That in turn enables high frequency operation. Furthermore, the switching frequency of SiC is much higher due to its high electron drift velocity.

High power handling and high switching frequencies of power devices increase the junction temperature. In comparison to Si and GaAs, SiC can operate in high temperature because of its wide bandgap as discussed earlier. Also, SiC has a much higher thermal conductivity in comparison to silicon and gallium arsenide that allows quick dissipation of generated heat to the environment, further lowering the temperature effect on the device.

1.2.3.3 Influence of radiation on SiC electrical properties

Semiconductors form acceptor or donor defects, also known as deep centers, upon exposure to radiation. These radiation-induced defects change the carrier density in the conduction band, which changes the conduction property of the material. For instance, in the case of acceptor defects, electron transfer from the conduction band to this defect results in a decrease in conductivity. Under extreme radiation doses, this process continues until a semiconductor eventually converts into an insulator. The process is commonly known as carrier (donor or acceptor) removal rate. The carrier removal rate of a semiconductor strongly depends on the threshold energy for defect formation under radiation. The threshold energy of a semiconductor can

Table 1.4 Calculated threshold energies of defect formation for Si, GaAS, Diamond, 3C-SiC, 4H-SiC and 6H-SiC.

Semiconductor	Si	GaAs	Diamond	3C-SiC	4H- and 6H-SiC
Lattice Constant, a_0 [Å]	5.65	5.431	3.57	4.36	3.08
Threshold Energy [eV]	9	12.8	80	37	153

be approximated using equation 1.11 [56]:

$$1.117E_d = (10/a_0)^{4.363} \tag{1.11}$$

where E_d is threshold energy of defect formation and a_0 is the lattice constant. The calculated threshold energies of defect formation for some common semiconductors are presented in Table 1.4.

Clearly from Table 1.4, 4H-SiC and 6H-SiC possess the highest radiation hardness among standard semiconductor substrate materials besides diamond, another contender for harsh environment electronics. Temperature also plays a vital role in radiation hardness of SiC as defect density decreases with increased temperature due to the high rate of recombination of primary defects at elevated temperatures.

1.2.3.4 Piezoresistance of SiC

Change in electrical resistance of a material when subjected to applied external stress is known as the piezoresistive effect. The effect has been used as a transduction mechanism for strain, pressure, and acceleration sensors. Typically the change in resistance is monitored by running a controlled current through the piezoresistor and monitoring voltage across the resistor. The sensor resistance changes due to an applied load, which causes a shift in voltage. The sensitivity of a piezoresistive sensor is quantified as gauge factor (GF), the percentage change in resistance per unit strain [57]. The relationship is given by equation 1.12:

$$GF = \frac{\Delta R}{R_0}\frac{1}{\varepsilon} \tag{1.12}$$

where R_0 is the nominal resistance of the network when no load is applied, ΔR is the change in resistance, and ε is the applied strain.

In addition, doping concentration, microstructure (single crystalline or polycrystalline), and operating temperature all have an effect on GF. At high temperature operation, piezoresistive transduction is affected by thermal stability, piezoresisitve gauge factor variation with temperature, and thermal coefficient of resistance of the material. Silicon is used in many piezoresistive transduction sensor applications owing to its high gauge factor [57, 58, 59]; however, poor thermal stability of silicon prevents its application to high temperature environments. SiC, in contrast, maintains a high gauge factor and is electrically and mechanically stable at high temperature.

Table 1.5 [60] Experimental room temperature gauge factor of n-type 3C-SiC at various resistivity levels and n-type silicon (©IEEE 1993), reprinted with permission.

Material	Resistivity	GF - π_{11}^*	GF - π_{12}^*	GF - $1/2(\pi_{11}+\pi_{12}+\pi_{44})^*$
n-type 3C-SiC	0.7	-31.8	19.2	-3.7
	0.02	-26.6		
	0.002	-12.7		
n-type silicon	11.0	133.0	68.3	-52

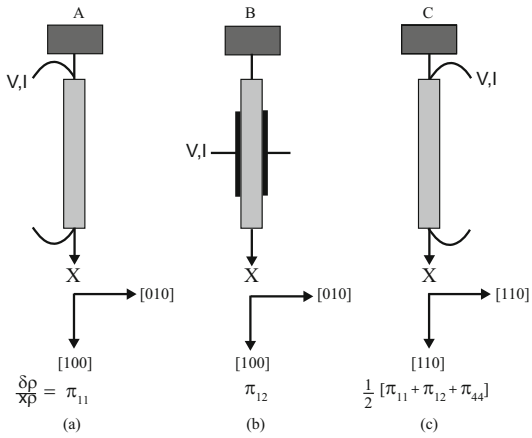

Fig. 1.13 [60] Schematic representation of strain gauges used to measure the GF of n-type 3C-SiC of different crystallographic orientations (©IEEE 1993), reprinted with permission.

Like silicon, the piezoresistance coefficient, and hence gauge factor, of SiC depends on the crystallographic orientation of the material. Table 1.5 lists the measured gauge factor of n-type 3C-SiC gauge factor at room temperature in comparison to n-type silicon. The GF corresponding to π_{11} has a larger value than the other coefficients, which means gauge orientation is a critical factor for maximizing sensitivity of 3C-SiC. On the other hand, the piezoresistance of 6H-SiC is isotropic within the base plane. Hence, the rotation of the gauge normal to the c-axis will not affect the gauge factor. Figure 1.13 shows schematically how metal foil strain gauges are placed to characterize the GF of different crystallographic orientations using a simple tension load test [60].

Although high gauge factor is important to improve strain sensitivity, thermal stability is also important to minimize aliasing of the sensor output to variations in temperature. For instance, Figure 1.14 shows the variation in GF for 3C-SiC with different resistivity values [60]. Although the higher resistivity layer exhibits a higher gauge factor, the lower resistivity layer maintains a decent GF yet exhibits very little shift in GF at operating temperatures above 500 K. This minimizes or eliminates the need for temperature compensation depending on the particular application requirements. Hence, 3C-SiC piezoresistive sensing is a viable load measurement technique in this temperature regime.

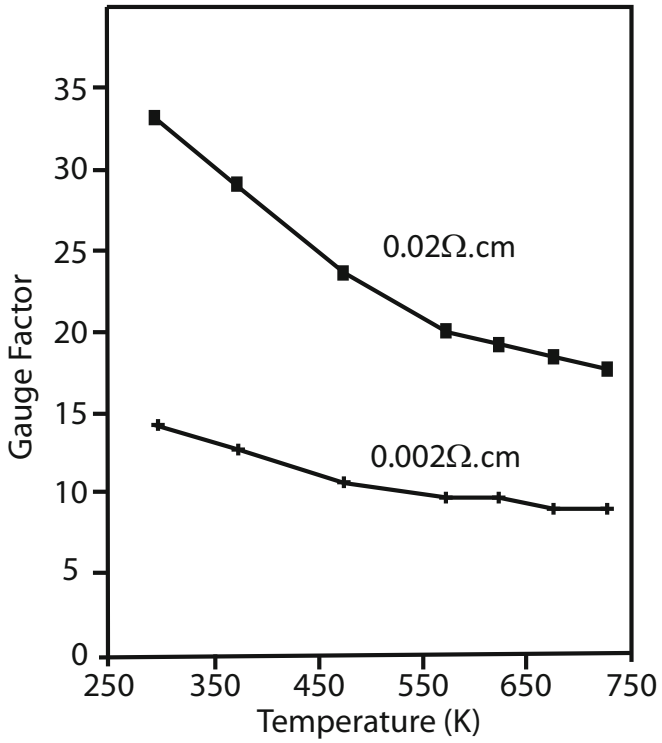

Fig. 1.14 [60] The gauge factor for single crystalline 3C-SiC with resistivity 0.02 and 0.002 Ω-cm as a function of temperature (©IEEE 1993), reprinted with permission.

1.2.4 Thermo-mechanical

Understanding mechanical properties is critical for designing sensors, actuators, and mechanical timing devices for applications in high temperature, high shock, and intense vibration conditions. Thermo-mechanical changes and shock- and vibration-induced stiction and fracture are considered the major failure mechanisms of micro-devices in the aforementioned conditions [61, 62, 63]. Thus, the thermo-mechanical stability, and the shock and vibration survivability are vital parameters in materials selection for harsh environment MEMS. This section reviews the thermo-mechanical properties of SiC.

The change in Young's modulus with temperature directly affects the performance of MEMS devices. This is true for static devices such as capacitive pressure and acceleration sensors as well as dynamic devices such as resonators. Based on recent studies of single crystalline 3C-SiC, the temperature coefficient of Young's modulus (TCYM) between room temperature and 800K is given by [66]:

$$E(T) = (-1.3 * 10^{-8} T^2 - 4.1 * 10^{-5} T + 1.0134) E_0 \tag{1.13}$$

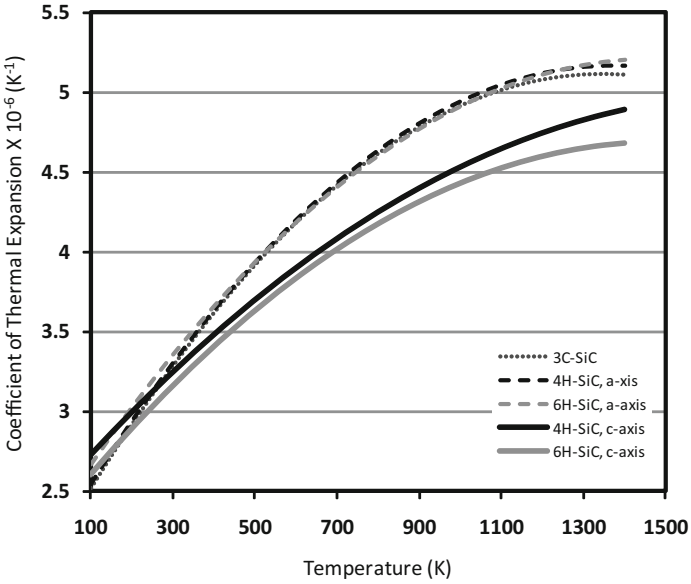

Fig. 1.15 CTE as a function of temperature of 3C-, 4H-, and 6H-SiC along their principle axis.

where E_0 is the Youngs modulus at room temperature.

Plastic deformation and changes in Young's modulus with temperature are the major parameters to consider when selecting materials for high temperature. The widely used MEMS material, Si, undergoes plastic deformation around 500 °C under minimal mechanical loads [64]. Hence, if high temperature operation is a requirement, silicon is not a viable option. Experimental data for 6H-SiC shows that macroscopic dislocation motion and plastic deformation starts above 1200 °C [65].

Furthermore, it is important to consider thermal expansion of SiC with changes in temperature (captured as a coefficient of thermal expansion, CTE). It is important because this expansion with temperature alters geometries or leads to stress changes in built-in beams when multiple material layers are used to form the device structure. In turn, this tends to change the response characteristics of a microstructure, aliasing the sensor response to the desired measurand. It is also important to note that often table values list a single value when typically CTE is a function of temperature. Figure 1.15 plots the CTE of 3C-, 4H-, and 6H-SiC along their principle crystal axes as a function of temperature [75]. Note that the CTE of SiC is significantly different whether the application is for room temperature or 600 °C, a shift in CTE of over 50%. It is also interesting to note that near room temperature the CTE of the various polytypes of SiC are actually close to the value for silicon.

Shock and vibration survivability is a fundamental requirement for most military and aerospace applications. MEMS devices can fail during shock and vibration due to two factors, stiction and fracture. Key material properties related to shock survival

Table 1.6 Bulk mechanical properties of select MEMS materials at 300 K [2, 63]. Note that some of the property values are from bulk material data. However, for feature size scales greater than 1 μm, the bulk material properties will be reasonably representative of the thin-film.

Property	Silicon	Silicon Nitride	Diamond	SiC
Young's modulus, E [GPa]	190	304	1035	448
Density, ρ [kg/cm^3]	2330	3300	3510	3300
Fracture Strength, σ_F [GPa]	2-4	5-8	8-10	4-10
E/ρ [GN/kg-m]	72	92	295	130

are listed in Table 1.6. Shock-induced stiction occurs when adjacent microstructures come into mechanical contact during the loading event. In general, materials with high E/ρ (stiffness-to-weight ratio) have reduced probability of stiction or fracture during a shock event because the high stiffness minimizes the defection while the low density decreases the magnitude of the inertial load. In terms of fracture failure, higher fracture strength is pivotal. SiC possesses higher fracture strength when compared to silicon and silicon nitride, only second to diamond; however, diamond is not as well suited for high temperature oxidative environments, as discuss previously.

1.3 System integration aspects of SiC materials

As discussed earlier in this chapter, SiC is an electronic semiconductor with a wide bandgap and high thermal conductivity, making it suitable for high power and high temperature operation. The wide band gap also reduces its sensitivity to radiation-induced damage. As a mechanical material for harsh environment MEMS, SiC possesses outstanding material properties, including high elastic stiffness and fracture toughness over silicon as well as stability of these properties beyond 500 °C. It also is chemically inert and resistant to wear. As will be discussed throughout the remainder of the book, SiC can be produced in various forms. They generally have similar mechanical and chemical properties yet have a variety of electrical properties and deposition temperatures, which will enable fabricating a variety of circuit elements and sensor structures.

Depending on the particular application and corresponding environmental constraints, integration complexity varies widely. Integration can be as simple as a micromachined device with an impedance matching buffer. It can be as complex as a micromachined device with control, sense, data processing, and communications electronics as well as on-board power supply. Integration of all major components of a microsystem (*i.e.*, electronics, sensors, and actuators) improves performance by reducing parasitics, increasing measurement sensitivity, reducing overall system size, and generally reduces power consumption. This high level of integration is also beneficial in reducing interconnect components, which further increases the opera-

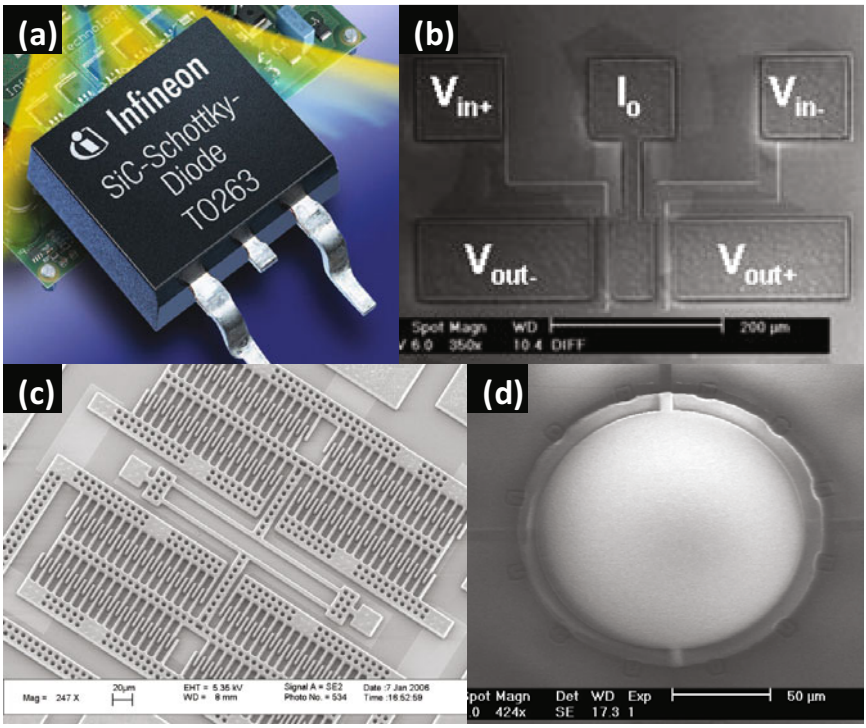

Fig. 1.16 (a) [70] picture of a commercial SiC Schottky diode from Infineon Inc., (b) [71] SEM micrograph of a 6H-SiC JFET based differential pair, (c) surface-micromachined 3C poly-SiC strain sensor, and (d) [67] SEM micrograph of a PECVD SiC encapsulated pressure sensor (©Elsevier 2003, Wiley-VCH Verlag GmbH & Co. KGaA 2009, and IOP 2004, respectively), reprinted with permission.

tional survivability in harsh environments since traditional interconnect technology is not typically suited for operation in corrosive or high temperature environments.

Figure 1.16 shows examples of discrete SiC devices fabricated using different forms of SiC (single-crystalline, epitaxial, polycrystalline and amorphous). These examples represent all major components of a microsystem: electronics, sensors, actuators, and packaging. From the materials point of view, not only the component but also the isolation and electrical routing layers must be fabricated using compatible materials. Compatibility in this case takes on several forms. First, the deposition methods must not damage previous layers, typically by not requiring excessively high deposition temperatures. Second, the coefficient of thermal expansion (CTE) differences between the various layers must be small because of the large operating temperature range expected for many of these harsh environment applications. Finally, both electrically insulative and conductive layers are needed and must meet the first two requirements in addition to withstanding the corrosive nature of the application in question.

Whether for high temperature operation or operation with frequent thermal cycling, one of the key areas of concern is CTE matching of every layer both at the discrete device level and system level. Thermal expansion differences between each layer as well as the substrate result in stresses during both fabrication and operation. In extreme cases, high thermal stress can lead to failure of the system due to delamination and cracking of the device layers [72]. These thermal stresses can also result in signal drift (unwanted thermal sensitivity). When the temperature-induced effects are large, passive or even active thermal compensation methods may not be able to successfully mitigate the problem [73, 74]. If the entire microsystem — substrate, electronics (including dielectrics), sensor components, and encapsulation — is produced only in SiC that would substantially reduce thermal mismatch as most forms of SiC have fairly similar CTE values. Thus, from the point of view of integrating a complete microsystem understanding CTE behavior of the complete material set is needed. To date, information available on CTE of poly-SiC and amorphous SiC is very limited. For both poly-SiC and amorphous SiC, deposition methods and specific conditions determine the microstructure of the resulting material, and the microstructure influences the CTE behavior. Thus, it is imperative to establish CTE data for poly-SiC and amorphous SiC based on deposition method and condition. This is one particular materials aspect that future research should focus on in order to realize complete SiC microsystem technology.

SiC can be produced in both electrically conductive and insulative forms. The conductivity of a SiC substrate can range from semi-insulating (10^5 Ω-cm) to highly conductive (0.028 Ω-cm) [68]. Doping concentration of the epitaxial SiC can be as high as $10^{19}/cm^3$. Poly-SiC can be produced with resistivity down to 0.02 Ω-cm while highly insulative amorphous SiC can be obtained by PVD and CVD methods [69]. Thus, it can be used as the primary platform for both mechanical device and electrical routing layers.

Utilizing the various forms of SiC for all aspects of the system would provide thermal, chemical, and mechanical stability for the entire system. Other materials with closely matched properties can also be considered for electrical and isolation layers. For example, silicon nitride and aluminum nitride are other possible isolation layer options for harsh environment applications since they both have closely matched CTE to SiC, can withstand high operating temperatures, and are fairly resistant to corrosion, although less so for silicon nitride.

This outlines the semiconductor technology aspects to integration. Integration of the many components goes well beyond the semiconductor properties alone. Issues such as compatibility of deposition and etching processes and thermal cycle influences on the electrical behavior of previously fabricated layers will be discussed along with fabrication techniques for SiC. Corrosion resistant metals that can make ohmic contact with SiC will be reviewed along with SiC-based electronics. Component interconnects will be explored when discussing SiC as a packaging material. At the end of the book, an overall approach is proposed that will take these various aspects of integration together as a whole to propose different integration schemes including a highly monolithic integration approach that simplifies piecewise integration of components and reduces system vulnerabilities to corrosive environments.

References

1. Kroetz GH, Eickhoff MH, Moeller H (1999). Silicon Compatible Materials for Harsh Environment Sensors. Sensors and Actuators 74:182–189
2. Mehregany M, Zorman CA, Rajan N, Wu CH (1998). Silicon Carbide MEMS for Harsh Environments. Proceedings of the IEEE 86(8):1594–1610
3. Hunter GW, Neudeck PG, Okojie RS, Beheim GM, Powell JA, Chen L (2003). An Overview of High-Temperature Electronics and Sensor Development at NASA Glenn Research Center. Journal of Turbomachinery 125:658–664
4. Sarro PM (2000). Silicon Carbide as a New MEMS Technology. Sensors and Actuators 82:210–218
5. Wright NG, Horsfall AB (2007). SiC Sensors: A Review. Journal of Physics D: Applied Physics 40:6345–6354
6. Hamada K (2009). Present Status and Future Prospects for Electronics in EVs/HEVs and Expectations for Wide Bandgap Semiconductor Devices. Materials Science Forum 600-603:889–893
7. Hillion M, Chauvin J, Grondin O, Petit N (2008). Active Combustion Control of Diesel HCCI Engine: Combustion Timing. USA Society of Automotive Engineers, Inc., Warrendale, PA:Report number 2008-01-0984
8. Yoon M, Lee K, Sunwoo M (2007). A Method for Combustion Phasing Control Using Cylinder Pressure Measurement in a CRDI Diesel Engine. Mechatronics 17:469–479
9. Toyota Motor Sales, USA Inc. Emissions #1 – Combustion Chemistry. http://www.autoshop101.com/forms/h55.pdf
10. Jurger RK (1999). Automotive Electronics Hadbook, McGraw-Hill, USA
11. Turner J (2009). Automotive Sensors. Momentum Press, New York
12. DeLaat JC, Chang CT (2003). Active Control of High Frequency Combustion Instability in Aircraft Gas-Turbine Engines. 16th International Symposium on Airbreathing Engines. Cleveland, Ohio, August 31-September 5, 2003:SABE2003–1054
13. He B, Shen T, Junichi K, Minggao O (2008). Input Observer-Based Individual Cylinder Air-Fuel Ratio Control: Modelling, Design and Validation. IEEE Transactions on Controls Systems Technology 16 (5):1057–1065
14. Minor RR, Rowe DW (1998).Utilization of GPS/MEMS-IMU for Measurement of Dynamics for Range Testing of Missiles and Rockets. Position Location and Navigation Symposium, IEEE 1998:602–607
15. Baum GA (1998). Manufacturing Process Control for Industry of the Future. National Academy Press, Washington, D.C. Publication NMAB-487-2
16. Kersey D (2000). Optical Fiber Sensors for Permanent Down Well Monitoring Applications in the Oil and Gas Industry. IEICE Transactions Electronics E83-C(3):400–404
17. Vandelli N (2008). SiC MEMS Pressure Sensors For Harsh Environment Applications. MicroNano News, April, 2008:10–12
18. Tschulena G (1988). Sensors for Process Control. Physica Scripta T23:293–298
19. Schadow KC (2004). MEMS Aerospace Applications. NATO Research and Technology Organization. RTO-EN-AVT-105
20. Brown TG, Davis B, Hepner D, Faust J, Myers C, Muller P, Harkins T, Hollis M, Miller C, Placzankis B (2001) Strap-Down Microelectromechanical (MEMS) Sensors for High-G Munition Applications. IEEE Transactions on Magnetics 37(1):336–342
21. Habibi S, Cooper SJ, Stauffer J-M, Dutoit B (2008). Gun Hard Inertial Measurement Unit Based on MEMS Capacitive Accelerometer and Rate Sensor. Position, Location and Navigation Symposium, 2008 IEEE/ION:232–237
22. Farrar CR, Worden K (2007). An Introduction to Structural Health Monitoring. Philosophical Transactions of Royal Society A 365:303–315
23. Eubank T (2007) Application of Condition Based Maintenance on Aerospace Structures. M.Sc. Thesis, Cranfield University
24. Romero R, Summers H, Cronkhite J (1996). NASA/CR-198446; ARL-CR-289

25. Beard SJ, Kumar A, Qing X, Chan HL, Zhang C, Ooi TK (2005) Practical Issues in Real-World Implementation of Structural Health Monitoring Systems. SPIE Smart Structures and Material Systems, San Diego CA, March 6-10, 2005:196–203
26. Cheng H (2007). Strategy for Assessment of WWER Steam Generator Tube Integrity. International Atomic Energy Agency. Report IAEA-TECDOC-1577
27. Kim I-S, Hong J-K, Kim H-N, Jang K-S (2003). Wear Behavior of Steam Generator Tubes in Nuclear Power Plant Operating Condition. Transactions of the 17th International Conference on Structural Mechanics in Reactor Technology (SMiRT 17), Prague, Czech Republic, August 1722, 2003:D04-5.
28. Wang GW, Pran K, Sagvolden G, Havsgard GB, Jensen AE, Johnson GA, Vohra ST (2001). Ship Hull Structure Monitoring Using Fibreoptic Sensors. Smart Materials and Structures 10:472–478
29. Chen H, Cardone V, Lacey P (1998). Use of Operation Support Information Technology to Increase Ship Safety and Efficiency. SNAME Transactions 106:105–127
30. Paik BG, Cho SR, Park B-J, Lee D, Yun J-H, Bae B-D (2007). Employment of Wireless Sensor Networks for Full-Scale Ship Application. IFIP International Federation for Information Processing, EUC 2007, LNCS 4808:113–122
31. Baldwin C, Kiddy J, Salter T, Chen P, Niemczuk J (2002). Fiber Optic Structural Health Monitoring System: Rough Sea Trials of the RV Triton. Oceans MTS/IEEE 3(3):1806–1813
32. Boller C (2001). Ways and Options for Aircraft Structural Health Management. Smart Materials and Structures 10:-432440
33. Gerardi TG (1990). Health Monitoring Aircraft. Journal of Intelligent Material Systems and Structures 1:375–384
34. Woelcken P, Bockenheimer C, Speckmann H, Entelmann W (2006). Outline of Overall Aircraft Imposed Requirements on Airframe Enhancements by Nanotechnologies and Resulting Opportunities. Proceedings of CANEUS 2006, August-September, Toulouse, France:69–72.
35. Staszewski WJ, Mahzan S, Traynor R (2009). Health Monitoring of Aerospace Composite Structures – Active and Passive Approach. Composites Science and Technology 69(11-12):1687–1685
36. Mancini S, Tumino G, Gaudenzi P (2006). Structural Health Monitoring for Future Space Vehicles. Journal of Intelligent Materials Systems and Structures 17:577–585
37. Derriso MM, Chang FK (2006). Future Roles of Structural Sensing for Aerospace Applications. NATO Research and Technology Organization: RTO-MP-AVT-141
38. Miller LM (1999). MEMS for Space Applications. SPIE Proceedings 3680:2–11
39. Tessler, A. (2007). Structural Analysis Methods for Structural Health Management of Future Aerospace Vehicles. NASA Report NASA/TM-2007-214871
40. Tor-Arne Grönland T-A, Pelle Rangsten P, Nese M, Lang M (2007). Miniaturization of Components and Systems for Space Using MEMS-Technology. Acta Astronautica 61:228–233
41. de Rooij RF, Gautsch S, Briand D, Marxer C, Mileti G, Noell W, Shea H, Staufer U, van der Schoot B (2009). MEMS for Space. Transducers 2009, Denver, CO, USA, June 21-25, 2009
42. Takahashi K (2004) Micro Thrusters for Miniaturized Space Systems, Need and Perspective. Power MEMS, Kyoto, Japan, Nov. 28-30, 2004:2–3
43. George T, Son KA, Powers RA, del Castillo LY, Okojie R (2005). Harsh Environment Microtechnologies for NASA and Terrestrial Applications. IEEE Sensors:1253-1258
44. Hunter GW, Okojie RS, Krasowski M, Beheim, GM, Fralick G, Wrbanek J, Greenberg, P, Neudeck PG, Xu J (2007). Microsystems, Space Qualified Electronics, and Mobile Sensor Platforms for Harsh Environment Applications and Planetary Exploration. 5th International Planetary Probe Workshop, Bordeaux, France, June 25-29, 2007.
45. Choyke WJ, Matsunami H, Pensl G (2004). Silicon Carbide: Recent Major Advances. Springer-Verlag, Berlin, Heidelberg, New York
46. Wijesundara MBJ, Valente G, Ashurst WR, Howe RT, Pisano AP, Carraro C, Maboudian R (2004). Single-Source Chemical Vapor Deposition of 3C-SiC Films in a LPCVD Reactor Part I: Growth, Structure, and Chemical Characterization. Journal of the Electrochemical Socciety 151:C210–C214.

47. Fu XA, Dunning JL, Zorman CA, Mehregany M (2005). Polycrystalline 3C-SiC Thin Films Deposited by Dual Precursor LPCVD for MEMS Applications. Sensors and Actuators A 119:169–176
48. Soloviev SI, Gao Y, Sudarshan TS (2000). Doping of 6H-SiC by Selective Diffusion of Boron. Applied Physics Letters 77(24):4004–4006
49. Zhuang D, Edgar JH (2005). Wet Etching of GaN, AlN, and SiC: a Review. Materials Science and Engineering 48:1–46.
50. Roper CS, Howe RT, Maboudian R (2009). Room-Temperature Wet Etching of Polycrystalline and Nanocrystalline Silicon Carbide Thin Films with HF and HNO_3. Journal of The Electrochemical Society 156(3):D104–D107
51. Wijesundara MBJ, Walther DC, Stoldt CR, Fu K, Gao D, Carraro C, Pisano AP, Maboudian R (2003). Low Temperature CVD SiC Coated Si Microcomponents for Reduced Scale Engines. Proceedings of ASME International Mechanical Engineering Congress and Exhibition, Washington D.C., November 15-21, 2003:IMECE2003-41696.
52. Fox DS, Opila EJ, Hann RE (2000). Paralinear Oxidation of CVD SiC in Simulated Fuel-Rich Combustion. Journal of American Ceramic Society 83(7):1761–1767
53. Neudeck PG (2006). Silicon Carbide Technology. The VLSI Handbook, Chapter 5 (Editor Wai-Kai Chen, CRC Press, Second Edition).
54. Patil AC (2009). Silicon Carbide JFET Integrated Circuit Technology for High-Temperature Sensors. Ph.D. Thesis. Case Western Reserve University.
55. Ozpineci B, Tolbert LM(2003). Comparison of Wide-Bandgap Semiconductors for Power Electronics Applications. ORNL/TM-2003/257
56. Lebedev AA, Kozlovski VV, Strokan NB, Davydov DV, Ivanov AM, Strel'chuk AM, Yakimova R (2002). Radiation Hardness of Wide-Gap Semiconductors (Using the Example of Silicon Carbide). Semiconductors 36(11):1270–1275
57. Kon S, Oldham K, Horowitz R (2007). Piezoresistive and Piezoelectric MEMS Strain Sensors for Vibration Detection. Proc. of SPIE Vol. 6529, Sensors and Smart Structures Technologies for Civil, Mechanical, and Aerospace Systems:65292V-1
58. French PJ, Evans AGR (1989). Piezoresistance in Polysilicon and its Applications. Solid-State Electronics 32(1):1–10
59. Suhling JC, Jaeger RC. Silicon Piezoresistive Stress Sensors and Their Application in Electronic Packaging. IEEE Sensors Journal 1(1):14–30
60. Shor JS, Goldstein D, Kurtz AD (1993). Characterization of n-Type β-SiC as a Piezoresistor. IEEE Transactions on Electron Devices 40(6):1093–1099
61. Srikar VT, Spearing SM (2003). Materials Selection in Micromechanical Design: An Application of the Ashby Approach. Journal of Microelectromechanical Systems 12(1):3–10
62. Srikar VT, Senturia SD (2002). The Reliability of Microelectromechanical Systems (MEMS) in Shock Environments. Journal of Microelectromechanical Systems 11(3):206–214
63. Spearing SM (2000). Materials Issues in Microelectromechanical Systems (MEMS). Acta Metallurgica 48:179–196.
64. Yonenaga I (2003). High-temperature Strength of Bulk Single Crystals of III-V Nitrides. Journal of Materials Science: Materials in Electronics 14:279–281
65. Yonenaga I (2001). Thermo-Mechanical Stability of Wide-Bandgap Semiconductors: High Temperature Hardness of SiC, AlN, GaN, ZnO and ZnSe. Physica B 308-310:1150–1152
66. Pozzi M, Hassan M, Harris AJ, Burdess JS, Jiang L, Lee KK, Cheung R, Phelps GJ, Wright NG, Zorman CA, Mehregany M (2007). Mechanical Properties of a 3C-SiC Film Between Room Temperature and 600 °C. Journal of Physics D: Applied Physics 40:3335–3342
67. Pakula LS, Yang H, Pham HTM, French PJ, Sarro PM (2004). Fabrication of a CMOS compatible pressure sensor for harsh environments. Journal of Micromechanics and Microengineering 14(11):1478–1483
68. Cree Semiconductor Product Specifications, www.cree.com
69. Wijesundara MBJ, Gao D, Carraro C, Howe RT, Maboudian R (2003). Nitrogen Doping of Polycrystalline 3C-SiC Films Grown Using 1,3-Disilabutane in a Conventional LPCVD Reactor. Journal of Crystal Growth 259:18–25

70. Telford M (2003). SiC's power cuts cost. III-Vs Review 16(4):44–47
71. Neudeck PG, Gaverick SL, Spry DJ, Chen L-Y, Beheim GM, Krasowsk MJ, Mehregany M (2009). Extreme temperature 6H-SiC JFET integrated circuit technology. Physica Solidi A 206(10):2329–2345
72. Savrun E (2002). Packaging Considerations for Very High Tepmerature Microsystems. Sensors 2002, June 12-14, 2002:1139–1143
73. Vig JR (2001). Temperature-Insensitive Dual-Mode Resonant Sensors – A Review. IEEE Sensors Journal 1:62–68
74. Melamud R, Kim B, Hopcroft MA, Chandorkar S, Agarwal M, Jha CM, Kenny TW (2007). Composite Flexural-Mode Resonator with Controllable Turnover Temperature. MEMS 2007, Kobe, Japan:199–202
75. Li Z,Bradt C (1986). Thermal Expansion of the Cubic (3C) Polytype of SiC. Journal of Materials Science 21:4366–4368